THE JOURNAL OF BIOLOGICAL CHEMISTRY VOL. 285, NO. 1, pp. 705–712, January 1, 2010

Hyperactive Intracellular Calcium Signaling Associated with Localized Mitochondrial Defects in Skeletal Muscle of an Animal Model of Amyotrophic Lateral Sclerosis*[S]

Received for publication, July 5, 2009, and in revised form, October 29, 2009 Published, JBC Papers in Press, November 4, 2009, DOI 10.1074/jbc.M109.041319

Jingsong Zhou[‡1], **Jianxun Yi**[‡], **Ronggen Fu**[§], **Erdong Liu**[§], **Teepu Siddique**[§], **Eduardo Ríos**[‡], **and Han-Xiang Deng**[§]

From the [‡]*Department of Molecular Biophysics and Physiology, Rush University Medical School, Chicago, Illinois 60612 and the* [§]*Department of Neurology, Northwestern University Feinberg School of Medicine, Chicago, Illinois 60611*

Amyotrophic lateral sclerosis (ALS) is a fatal neuromuscular disorder characterized by degeneration of motor neurons and atrophy of skeletal muscle. Mutations in the superoxide dismutase (SOD1) gene are linked to 20% cases of inherited ALS. Mitochondrial dysfunction has been implicated in the pathogenic process, but how it contributes to muscle degeneration of ALS is not known. Here we identify a specific deficit in the cellular physiology of skeletal muscle derived from an ALS mouse model (G93A) with transgenic overexpression of the human $SOD1^{G93A}$ mutant. The G93A skeletal muscle fibers display localized loss of mitochondrial inner membrane potential in fiber segments near the neuromuscular junction. These defects occur in young G93A mice prior to disease onset. Fiber segments with depolarized mitochondria show greater osmotic stress-induced Ca^{2+} release activity, which can include propagating Ca^{2+} waves. These Ca^{2+} waves are confined to regions of depolarized mitochondria and stop propagating shortly upon entering the regions of normal, polarized mitochondria. Uncoupling of mitochondrial membrane potential with FCCP or inhibition of mitochondrial Ca^{2+} uptake by Ru360 lead to cell-wide propagation of such Ca^{2+} release events. Our data reveal that mitochondria regulate Ca^{2+} signaling in skeletal muscle, and loss of this capacity may contribute to the progression of muscle atrophy in ALS.

ALS[2] is a neuromuscular disease characterized by degeneration of motor neurons and muscle atrophy. Mutations in the superoxide dismutase (SOD1) gene are associated with ~20% of inherited ALS cases and represent the most prevalent cause for familial ALS (1). Transgenic mice with overexpression of ALS-associated human SOD1 mutations develop syndromes similar to those of human ALS patients (2). Numerous studies using ALS transgenic models show that accumulations of mutant SOD1 inside mitochondria are likely the cause of the functional impairments in motor neurons (reviewed in Ref. 1). Morphological and biochemical analyses reveal defective mitochondria in skeletal muscle of ALS patients (reviewed in Ref. 3), which are also observed in the ALS transgenic models (4–7). Although many studies are focused on the neurodegenerative aspect of ALS, the function of defective mitochondria in muscle degeneration during ALS progression has not been extensively examined.

Muscles use Ca^{2+} as a messenger to control events ranging from activation of contraction to cell death. Defective intracellular Ca^{2+} signaling and homeostasis have been linked to skeletal muscle dysfunction during aging (8, 9) and in muscular dystrophy (*mdx*) (10–14). In skeletal muscle, Ca^{2+} release and uptake are mainly controlled by the sarcoplasmic reticulum (SR), which forms a network that is intimately associated with the mitochondria organelle. This close spatial proximity between SR and mitochondria, together with the ability of mitochondria to take up Ca^{2+} from the cytosol, suggests that mitochondria could play an important role for modulating intracellular Ca^{2+} signaling in muscle cells (reviewed in Ref. 15). Whether mitochondrial Ca^{2+} uptake modulates physiological Ca^{2+} transients in skeletal muscle and whether alteration of the mitochondrial Ca^{2+}-buffering capacity contributes to muscle dysfunction in pathophysiological conditions are unresolved questions.

Here we examine mitochondrial function and Ca^{2+} signaling in skeletal muscle derived from $SOD1^{G93A}$ transgenic mice (G93A) (2). In the G93A muscle, we identify localized defects in mitochondrial structure and function that are associated with hyperactive Ca^{2+} release from the SR at the lesion site. The muscle fiber segments with defective mitochondria appear at the neuromuscular junction (NMJ) region and are found in young mice prior to the onset of overt disease. Our data suggest that myogenic defects in mitochondria-mediated control of SR Ca^{2+} release can potentially contribute to the progression of muscle wasting in ALS.

EXPERIMENTAL PROCEDURES

Animals and Isolation of Single Muscle Fibers—G93A mice were maintained in the C57B6XSJL background, and age-matched wild type C57B6XSJL mice were purchased from The Jackson Laboratory. G93A mice at the age of 1 month

* This work was supported in whole by Research Grant MDA4351 from the Muscular Dystrophy Association (to J. Z.) and in part by National Institutes of Health Grants AR032808 and AR049184 (to E. R.) through NIAMS and NS050641 and NS046535 (to T. S.) and NS040308 (to H. X. D.) through NINDS.

[S] The on-line version of this article (available at http://www.jbc.org) contains supplemental data 1 and data 2.

[1] To whom correspondence should be addressed: 1750 W. Harrison St., Chicago, IL 60612. Tel.: 312-942-8044; Fax: 312-942-8711; E-mail: jzhou1@rush.edu.

[2] The abbreviations used are: ALS, amyotrophic lateral sclerosis; FCCP, carbonyl cyanide *p*-trifluoromethoxyphenylhydrazone; FDB, flexor digitorum brevis; NMJ, neuromuscular junction; SOD1, superoxide dismutase type I; SR, sarcoplasmic reticulum; TMRE, tetramethylrhodamine ethyl ester; WT, wild type.

(presymptomatic stage) and 3–4 months (stage of disease onset with apparent ALS symptoms) (2) were used in this study. Individual muscle fibers were isolated from these mice following the protocol of Wang *et al.* (12). Briefly, flexor digitorum brevis (FDB) muscles were digested in modified Krebs solution (no Ca^{2+}) plus 0.2% type I collagenase for 55 min at 37 °C. Following collagenase treatment, the muscle fibers were stored in the enzyme-free Krebs solution at 4 °C and used for functional studies within 36 h.

Fluorescent Dye Loading and Confocal Microscopic Imaging of Muscle Fibers—FDB muscle fibers were incubated with 500 nM MitoTracker Deep Red and 50 nM tetramethylrhodamine ethyl ester (TMRE) for 10 min at 25 °C. Confocal microscopy was used for visualization of mitochondrial morphology and membrane potential ($\Delta\Psi$). For simultaneous monitoring of $\Delta\Psi$ and intracellular Ca^{2+} concentration ($[Ca^{2+}]_i$), muscle fibers were first incubated with 3 μM fluo-4 AM for 60 min and then incubated with 50 nM TMRE for 10 min. In separate studies, α-BTX (bungarotoxin conjugated with Alexa Fluor 647, 1.5 mg/ml, 10 min at 25 °C) was used to label the NMJ area in single fibers. For quantification of resting $[Ca^{2+}]_i$, muscle fibers were incubated with 3 μM indo-1 AM for 2 h at 25 °C. Confocal images were collected in SEER mode (16) using the scanner SP2-AOBS with ×63, 1.2 NA water-immersion objective lens (Leica Microsystems). Chemicals were purchased from Sigma, fluorescent dyes were from Invitrogen, and Ru360 was from Calbiochem.

Live Cell Imaging of Osmotic Stress-induced Local Ca^{2+} Release in Muscle Fibers—Muscle fibers loaded with indicators of $[Ca^{2+}]_i$ (fluo-4 AM) and $\Delta\Psi$ (TMRE) in Krebs solution were exposed to a 170 mosM hypotonic solution containing (in mM) 64 NaCl, 5 KCl, 10 Hepes, 10 glucose, 2.5 $CaCl_2$, 2 $MgCl_2$, pH 7.2, for 2 min and then returned to Krebs solution. Ca^{2+} signals were monitored before, during, and after the osmotic shock following the protocol developed by Wang *et al.* (12).

Image Processing and Data Analysis—iTool (IDL, ITT Visual Information Solutions) was used to display the images and to measure the average fluorescence intensity in regions of interest within muscle fibers. Averages over different fibers (or fiber regions) are represented as mean ± S.E. Statistical significance was determined using Student's *t* test.

Transmission Electron Microscopy—FDB muscles were dissected and pinned down to a Sylgard dish in Krebs solution. After removing the connective tissue, the muscle was fixed in 0.1 M sodium cacodylate, pH 7.4, plus 4% paraformaldehyde and 2.5% glutaraldehyde for 4 h at room temperature. Fixed samples were embedded using standard techniques. Ultrathin sections were cut by diamond knife and examined by electron microscopy (17).

RESULTS

ALS Muscle Fibers Show Depolarized Mitochondria near NMJ—Individual FDB muscles isolated from G93A mice and age-matched wild-type (WT) controls were used for structural and functional studies. Using electron microscopy, we found that in WT muscle, most mitochondria are of uniform size and are located within the sarcomeric I band (Fig. 1*A*, *panel 2*), a pattern that is similar to previous studies (8, 15). The G93A muscle displayed abnormal mitochondria that can appear within the sarcomeric A band (Fig. 1*A*, *panel 1*). Some mitochondria in G93A muscle display internal vacuoles (Fig. 1*A*, *panels 3–5*), as has been previously reported in the motor neurons of ALS transgenic mice (18, 19).

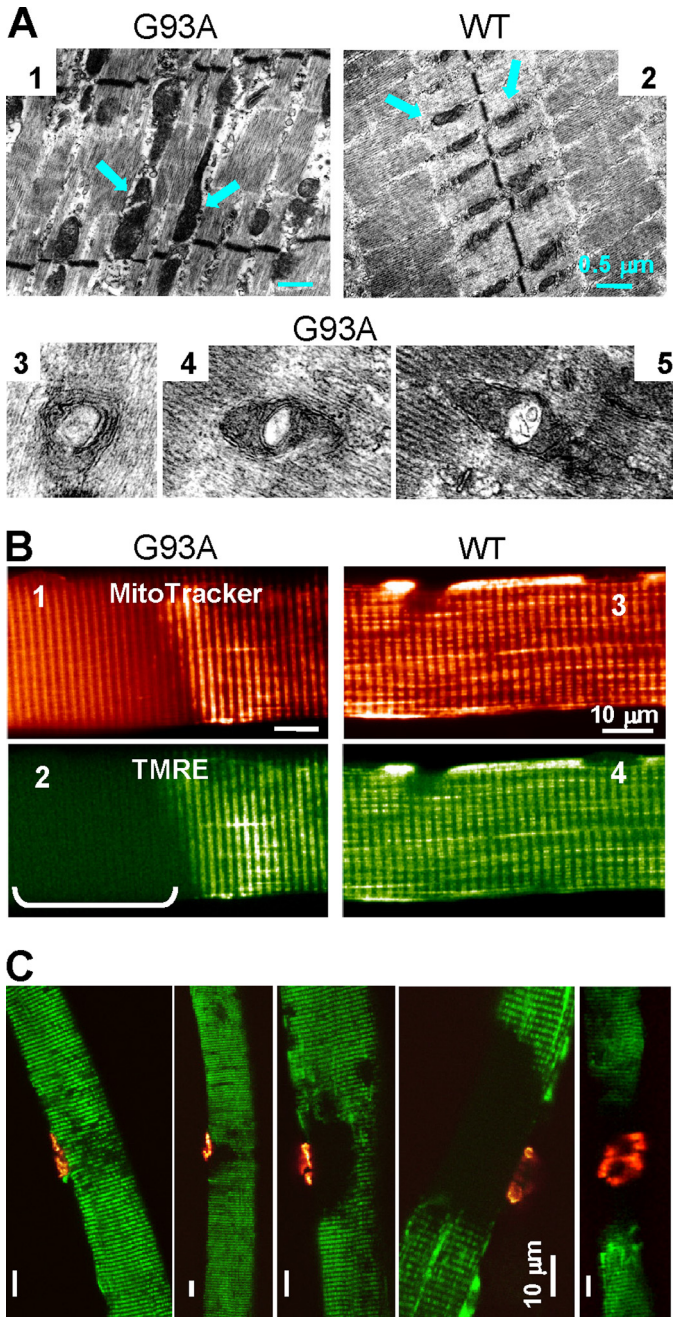

FIGURE 1. **Structural and functional defects of mitochondria in G93A muscle.** *A*, electron microscopy images of FDB muscles from 3-month-old G93A and WT mice. In the WT, mitochondria (*arrows*) aligned within the sarcomeric I band and had uniform sizes (*panel 2*). In contrast, G93A muscle (*panel 1*) had enlarged mitochondria with vacuoles (*panels 3–5*), invading the sarcomeric A band. *B*, live muscle fibers probed simultaneously with MitoTracker Deep Red (*panels 1* and *3*) and TMRE (*panels 2* and *4*). A segment with depolarized mitochondria is identified in the G93A fiber (*panel 2, bracket*). The corresponding segment in the MitoTracker Deep Red image shows fuzzy staining with loss of contrast, due to morphological alterations of mitochondria (*panel 1*). Both mitochondrial probes stain the WT fiber equally and homogeneously (*panels 3* and *4*). *C*, overlays of TMRE (*green*) and α-BTX images (*red*) of dually stained G93A FDB fibers. Areas of mitochondrial defects had variable size, but they always faced the NMJ.

For live-cell imaging of mitochondrial morphology and membrane potential, FDB fibers were simultaneously incubated with MitoTracker Deep Red and TMRE. MitoTracker Deep Red stains the mitochondrial network, and TMRE is a voltage-sensitive fluorescent indicator for mitochondrial transmembrane potential, $\Delta\Psi$. The distribution patterns for MitoTracker Deep Red and TMRE are uniform in WT muscle (Fig. 1*B*, *panels 3* and *4*). In contrast, the G93A muscle fiber displays localized defects in mitochondria, as shown by the regional loss of TMRE staining (Fig. 1*B*, *panel 2*) and fuzzy labeling by MitoTracker Deep Red at the same fiber segment (Fig. 1*B*, *panel 1*). This alteration in TMRE staining suggests substantial loss of $\Delta\Psi$ in the affected region. 10–60% of the muscle fibers isolated from G93A mice at the age of disease onset (3–4 months) showed depolarized mitochondria in fiber segments of various lengths ($n = 20$ mice). This phenotype was rarely observed in the age-matched WT mice. Such defective mitochondria were also observed in four young G93A mice investigated at the age of 37 days but not in WT mice at the same age ($n = 4$). This finding constitutes the first evidence of specific defects in mitochondrial structure and function in live muscle fibers of transgenic ALS mice that can occur prior to onset of neurodegeneration and muscle atrophy.

To determine whether the observed mitochondrial defect in G93A fibers was associated with NMJ, we simultaneously imaged the mitochondrial lesion and the NMJ by staining live G93A muscle fibers with TMRE and α-BTX, a ligand of the nicotinic acetylcholine receptor in postsynaptic membranes. As shown in Fig. 1*C*, although the size of affected segments with depolarized mitochondria varied among fibers, in every case ($n = 50$), the fiber segments with depolarized mitochondria always included the muscle side of the NMJ. Thus, the localized mitochondrial defect at the NMJ is a distinct phenotype of the ALS muscle. This defect may represent an early event in the pathogenesis of ALS.

Hyperactive Ca^{2+} Release in Fiber Segments with Depolarized Mitochondria—The finding of localized mitochondrial defects in G93A fibers presents a unique opportunity to test whether changes in mitochondrial function can affect intracellular Ca^{2+} signaling as we can compare Ca^{2+} release activity in regions with or without depolarized mitochondria in the same muscle fiber. For this purpose, we used osmotic stress-induced Ca^{2+} sparks as an index for the integrity of the intracellular Ca^{2+} release machinery (8, 12, 20–22). Intact FDB fibers isolated from G93A and WT mice were loaded with fluo-4 AM and TMRE for measurement of intracellular Ca^{2+} release and simultaneous monitoring of mitochondrial $\Delta\Psi$. In the resting condition, spontaneous Ca^{2+} sparks were rarely observed in G93A or WT cells. Transient exposure of muscle fibers to a hypotonic solution caused cell swelling in both WT and G93A muscle fibers and frequent Ca^{2+} release events upon return to isotonic solution (Fig. 2). In the WT muscle, the mitochondria were uniformly labeled by TMRE, indicating normal polarization of mitochondrial membranes (Fig. 2*A*, *panel 1*). Consistent with previous observations (12, 20), the osmotic stress-induced Ca^{2+} sparks were confined to the peripheral region of the WT fiber. In contrast, G93A fibers displayed more frequent Ca^{2+} release events that were not restricted to the periphery of the

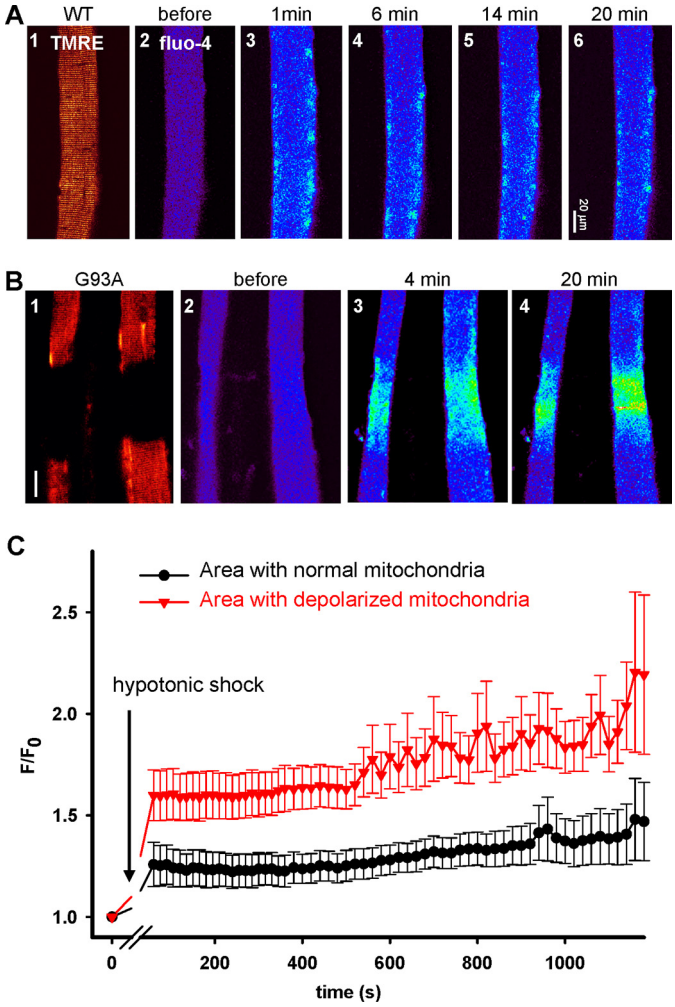

FIGURE 2. **Hyperactive Ca^{2+} release in G93A muscle fibers.** *A*, the response of a WT fiber to osmotic shock. TMRE stains the entire fiber homogeneously (*panel 1*). Osmotic stress-induced Ca^{2+} release events (after *panel 2*) are mainly confined to the peripheral region of the fiber. *B*, the responses of G93A fibers. Lack of TMRE staining identifies fiber segments with depolarized mitochondria (*panel 1*). The shock-induced Ca^{2+} release activity was greater and not restricted to the periphery of the fiber in the segments with depolarized mitochondria (*panels 3* and *4*). *C*, evolution of fluo-4 fluorescence in regions with normal or defective mitochondria in G93A muscle fibers. Mean (±S.E. (*error bars*)) over experiments of area-averaged fluorescence, normalized to values before the osmotic shock, is shown. The difference between normal and lesioned areas was highly significant ($n = 6$, $p < 0.0001$).

G93A fiber, specifically within areas of the muscle fiber that had defective TMRE labeling (Fig. 1*B*, *panels 3* and *4*). These hyperactive Ca^{2+} release events are similar to those observed in *mdx* muscle (12), suggesting that ALS muscle may share features with dystrophic phenotypes.

For quantitative comparison, the fluorescence intensity of fluo-4 in G93A muscle fibers was averaged in regions with normal or depolarized mitochondria. The mean of these averages over six completed experiments is plotted in Fig. 2*C*. Clearly, the defective regions responded to osmotic shock with greater local increase in cytosolic Ca^{2+}. Greater increase in cytosolic Ca^{2+}, likely caused by greater Ca^{2+} release in response to stimuli in regions with depolarized mitochondria, appears to be a characteristic feature of the affected muscle in the ALS mouse model. This Ca^{2+} regulatory defect is likely to result from mitochondrial defects. Indeed, we examined the rest-

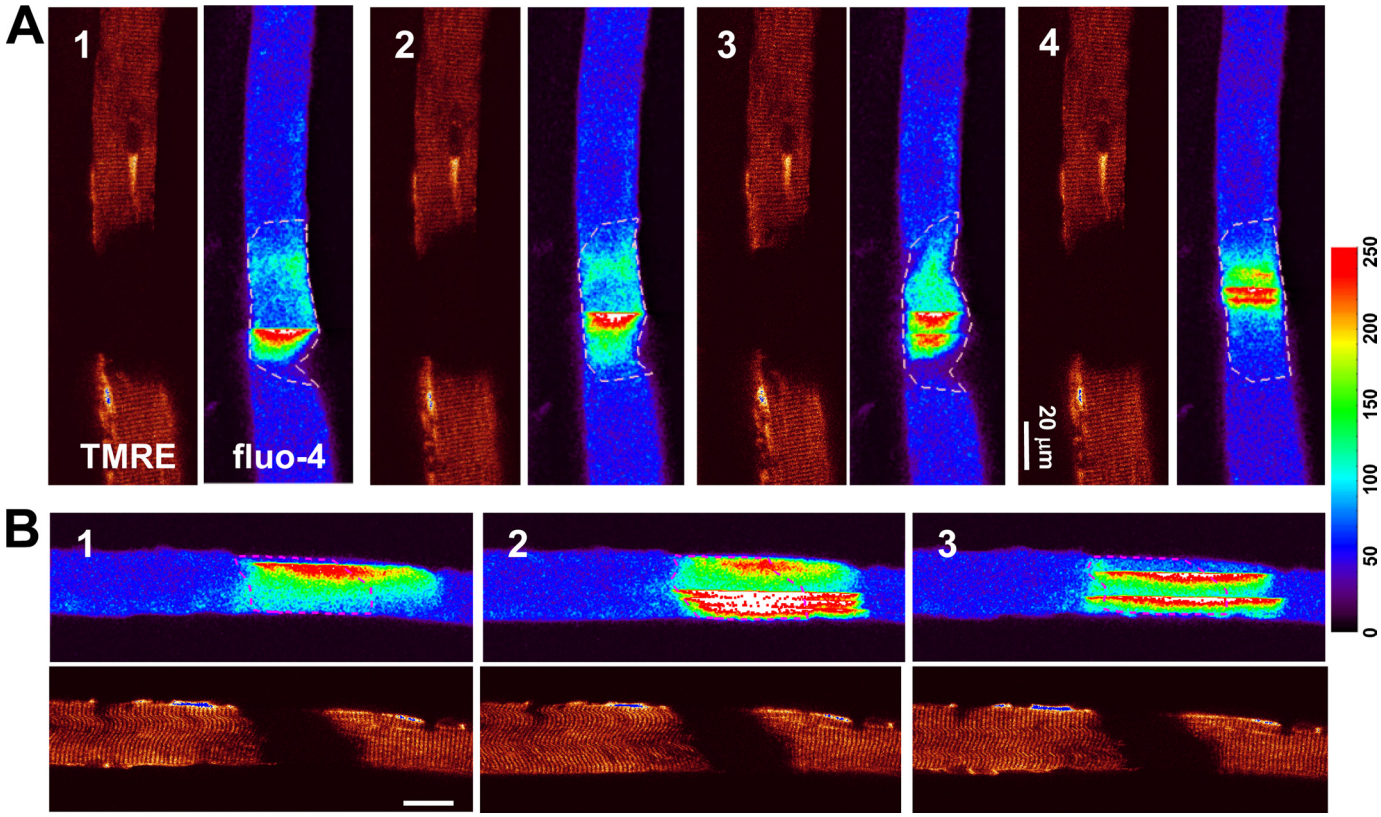

FIGURE 3. **Stress-induced Ca^{2+} waves stop in the region with normal mitochondria.** Images of $\Delta\Psi$ (TMRE) and cytosolic $[Ca^{2+}]_i$ (fluo-4) simultaneously obtained in G93A fibers are shown. *A*, transversely scanned *xy* images (with the rapidly changing abscissa *x* perpendicular to the fiber axis), showing Ca^{2+} waves for the 20 min following the osmotic shock. Ca^{2+} waves occur only in the region with depolarized mitochondria. *B*, longitudinally scanned images, with abscissa *x* along the fiber axis. Ca^{2+} waves invade the normal region for not more than ~30 μm.

ing cytosolic $[Ca^{2+}]$ ($[Ca^{2+}]_i$) using indo-1 (23) and found no significant change (168.2 ± 10.2 nM, n = 26 for WT; 175.7 ± 7.4 nM, n = 27 for G93A). This finding suggests that the interplay of the plasma membrane transport functions that determine resting $[Ca^{2+}]_i$ is not affected by expression of the $SOD1^{G93A}$ mutant in muscle. It also rules out a direct action of increased resting $[Ca^{2+}]_i$ as a cause of the hyperactive release in the mutant cells.

Areas with Polarized Mitochondria Stop the Propagation of Ca^{2+} Waves—Local defects in mitochondrial $\Delta\Psi$ reduce the driving force for Ca^{2+} uptake, and loss of the Ca^{2+}-sequestering capacity of mitochondria may underlie the hyperactive Ca^{2+} release observed within the defective region in the G93A fibers. A reduced mitochondrial Ca^{2+} uptake in the presence of random activation of Ca^{2+} release channels might allow individual channel openings to progress to a local release event or spark via recruitment of neighboring channels by Ca^{2+}-induced Ca^{2+} release (24). If this was the case, one would predict that normally polarized mitochondria play a basal containment role to prevent local activation and otherwise control Ca^{2+} release responses. More support for these views was obtained from the following observations.

Although WT muscle does not show Ca^{2+} waves at rest or even after osmotic shock (12, 22), we found that a portion of the G93A muscle fibers showed Ca^{2+} waves after osmotic stress (Fig. 3*A*). These Ca^{2+} waves often originated in regions with depolarized mitochondria and never appeared elsewhere in the muscle fiber with normal mitochondrial potential. Fig. 3*B* shows longitudinal scan images of a G93A muscle fiber, which allows comparing the evolution of Ca^{2+} waves in areas with different mitochondrial polarization. Clearly, Ca^{2+} waves that originate within the segment with depolarized mitochondria can only penetrate into the nearby normal region for distances of less than 30 μm (n = 4). The limited propagation of Ca^{2+} waves in areas with normal mitochondria of the G93A muscle suggests that mitochondria with polarized membrane may have the ability to take up Ca^{2+} at a rate that is sufficient to stop the propagation of Ca^{2+} waves.

Inhibition of Mitochondrial Ca^{2+} Uptake Exacerbates the Hyperactive Ca^{2+} Release—Pharmacological assays were conducted to test whether reduced mitochondrial Ca^{2+} uptake underlies the hyperactive Ca^{2+} release activity in G93A muscle. To reduce the driving force of mitochondrial Ca^{2+} uptake, we used FCCP, a proton ionophore that collapses $\Delta\Psi$. Oligomycin (200 nM) was added to block the reverse activity of mitochondrial ATP-synthase and thereby slowed down the depletion of ATP during FCCP application. Fig. 4*A* shows representative images of cytosolic Ca^{2+} and TMRE staining in a time series. Following osmotic stress, the muscle fiber segment with defective mitochondrial potential (as revealed by the reduced TMRE labeling, Fig. 4*A*, *panel 1*) produced more Ca^{2+} release events than the normal region where the staining by TMRE was strong (Fig. 4*A*, *panels 2* and *3*). After the application of FCCP (1 μM), Ca^{2+} release events with increased frequency and intensity were observed that expanded into fiber segments originally

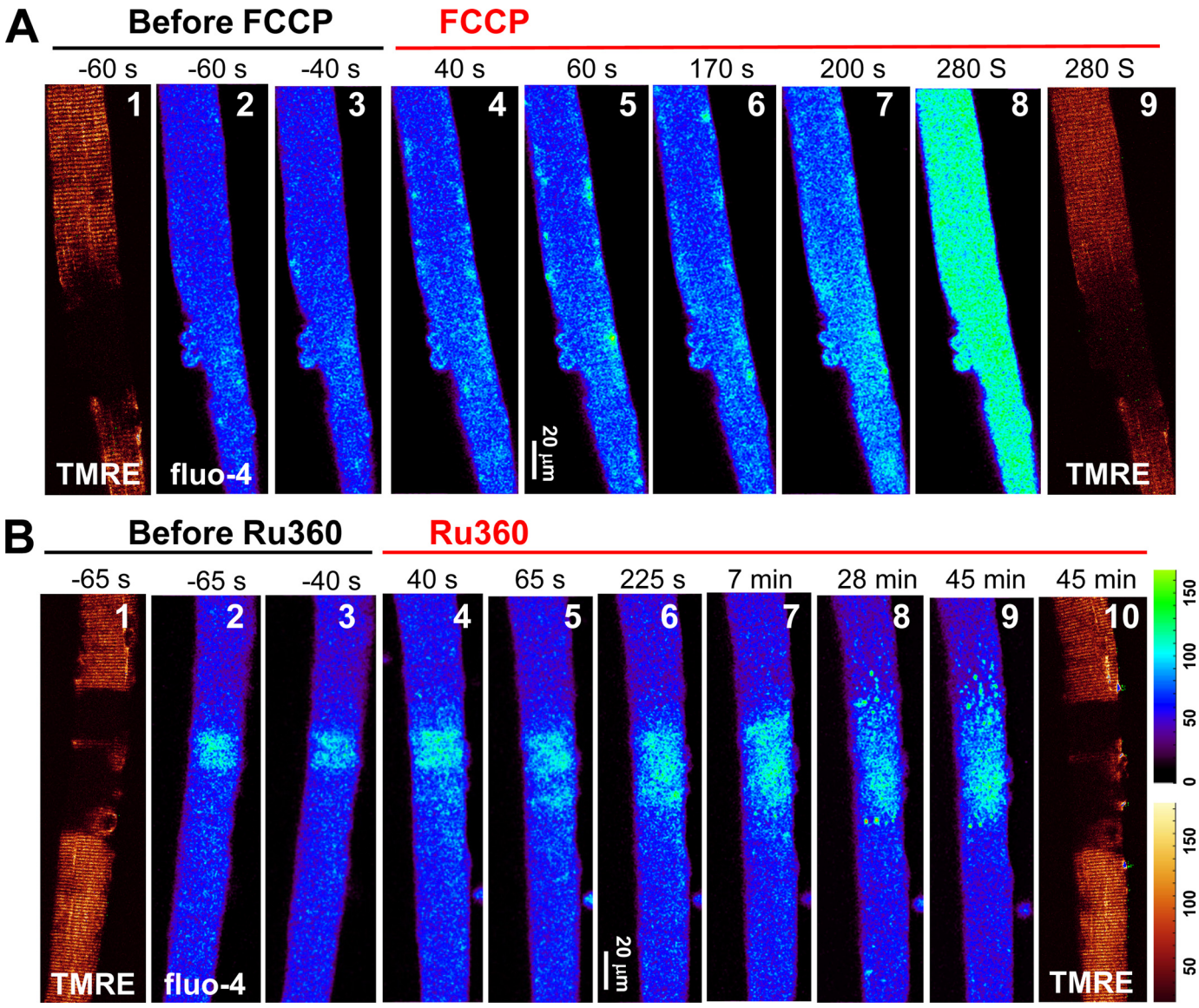

FIGURE 4. **Blocking mitochondrial Ca^{2+} uptake by FCCP and Ru360.** *A*, Ca^{2+} release events triggered by osmotic shock (*panels 2* and *3*). The application of FCCP (1 μM, added 5 min after the shock) caused an increase in Ca^{2+} events (*panels 4–7*). At 280 s, Ca^{2+} release engulfed the entire fiber (*panel 8*). TMRE staining in the normal areas also decreased (*panel 9*). *B*, increased Ca^{2+} release activity in a G93A fiber after the application of Ru360 (*panels 4–9*). The mitochondrial potential was not changed by Ru360 after 45 min (*panel 10*).

with normal mitochondria (Fig. 4*A*, *panels 4–7*), leading to global elevation of cytosolic Ca^{2+} (Fig. 4*A*, *panel 8*). The reduced TMRE staining after FCCP treatment (Fig. 4*A*, *panel 9*) confirms the reduction of $\Delta\Psi$, concomitant with widespread increase in Ca^{2+} release activity. After 5 min of FCCP exposure, the averaged fluorescence of TMRE in the normal region decreased to 0.61 ± 0.16 of control, whereas the averaged fluorescence of fluo-4 increased 2.17 ± 0.60-fold ($n = 8$, $p < 0.001$).

We then used Ru360, a specific blocker of the mitochondrial Ca^{2+} uniporter (25), to see whether direct inhibition of mitochondrial Ca^{2+} uptake can affect the propagation of Ca^{2+} release in G93A muscle fibers. As shown in Fig. 4*B*, active osmotic stress-induced Ca^{2+} release events were restricted to the region with depolarized mitochondria (Fig. 4*B*, *panels 2* and *3*). The application of 20 μM Ru360 caused an immediate increase in Ca^{2+} release activity (Fig. 4*B*, *panels 4–6*). Previous studies have shown that Ru360 can have a biphasic effect on mitochondrial Ca^{2+} uptake in cardiac myocytes, with a slow onset that requires a prolonged incubation of 28 min (26). When recording was extended to longer times after Ru360 application (Fig. 4*B*, *panels 7–9*), we observed a further increase in Ca^{2+} release, resulting in elevation of fluorescence to 1.25 of control level after 30 min ($n = 4$, $p = 0.08$). The mitochondrial potential was not changed even after 45 min in Ru360 (Fig. 4*B*, *panel 10*), confirming that the mildly increased Ca^{2+} release activity was due to block of the Ca^{2+} uptake pathway. In comparison with the effect of FCCP (Fig. 4*A*), global elevation of cytosolic Ca^{2+} was never observed even with the prolonged application of Ru360. One possible explanation for the lesser effect of Ru360 is the presence of other pathways of Ca^{2+} uptake, including a rapid mode of mitochondrial Ca^{2+} uptake that is less sensitive than the uniporter to ruthenium red (27).

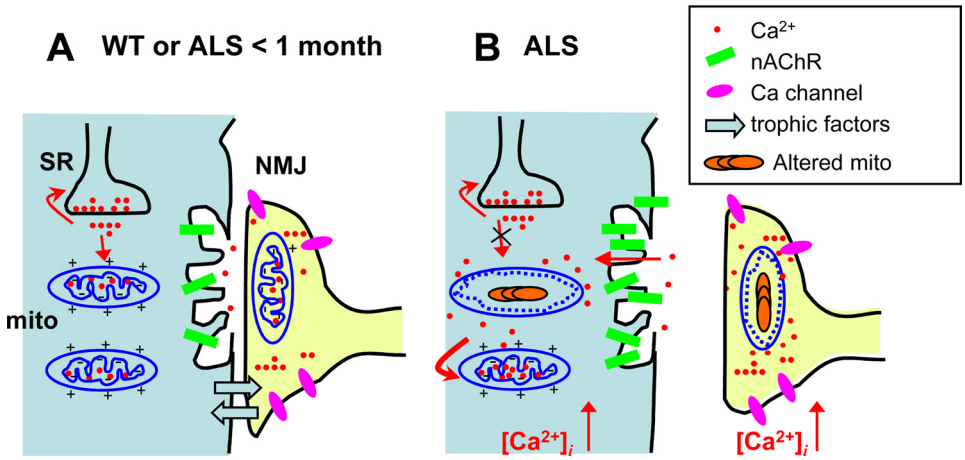

FIGURE 5. **Proposed pathogenic sequence in muscle of the ALS mouse model.** *A*, in the early presymptomatic stages, the situation is similar to the WT. *mito*, mitochondria. *B*, accumulation of mutant SOD1 inside mitochondria results in functional deficits, including a reduced $\Delta\Psi$ and Ca^{2+} removal by mitochondria. The alterations lead to progressive withdrawal of the nerve terminal. These changes can be self-reinforcing consequences, including loss of mutual trophic signals between muscle and nerve cells, uncontrolled release of Ca^{2+} from the SR, local cytosolic and mitochondrial increase in $[Ca^{2+}]$ (in both cells), and more Ca^{2+} stress on the normal mitochondria. The process may be characterized as a dual interplay between abnormal mitochondria and uncontrolled SR and between muscle fibers and altered nerve terminals, which eventually leads to destruction of both cells. *nAChR*, nicotinic acetylcholine receptor.

DISCUSSION

In this study, we show that muscle fibers derived from the ALS mouse model exhibit localized mitochondrial defects characterized by altered structure and loss of membrane potential, which is accompanied by an increased tendency to release stored Ca^{2+} from the SR. The increased activity of Ca^{2+} release is restricted to the area of compromised mitochondrial membrane potential, and pharmacological inhibition of mitochondrial Ca^{2+} uptake exacerbates this abnormal activity, suggesting that a deficit of mitochondrial Ca^{2+} uptake is likely a cause of the augmented Ca^{2+} release activity in the G93A muscle. We also find that Ca^{2+} waves that start from the defective region in G93A muscle could not propagate much inside the regions with normally polarized mitochondria, revealing the strong mitochondrial buffering capacity of Ca^{2+} released from the SR. Loss of this mitochondrial control of intracellular Ca^{2+} may constitute a significant step in the progression of muscle atrophy in ALS.

These results provide the first evidence that the mitochondrial lesion appears first at the NMJ region in the G93A muscle and is an early event of ALS progression. ALS has been described as a "distal axonopathy," which affects the axon and NMJ in G93A mice at the age of 47 days, prior to significant loss of neuronal bodies and the onset of muscle atrophy (28). One of the matters in dispute is the importance of denervation as a pathogenic event contributing to muscle atrophy. The initial defect on the muscle side of the NMJ may reflect the early consequences of denervation. However, this mitochondrial lesion appears in G93A muscle at the age of 37 days, before axonal withdrawal is expected to occur. Therefore, one aspect of the muscle pathology in ALS could result from intrinsic defects in the mitochondria of skeletal muscle.

The NMJ conducts retrograde signals from muscle to nerve, which play critical roles in axonal growth and maintenance of synaptic connections in adult motor neurons (29, 30). It was previously found that expression of a muscle-specific insulin-like growth factor 1 (Igf-1) isoform in the G93A model enhanced motor neuronal survival and could delay the progression of the disease (31). A primary muscle effect is supported by a recent study of Dobrowolny *et al.* (32), who found that muscle-restricted expression of $SOD1^{G93A}$ directly caused muscle atrophy and mitochondrial dysfunction. Their electron microscopy study revealed swelling mitochondria with vacuoles similar to those that we observed in the muscle of G93A mice, suggesting the possibility that SOD1 mutation-mediated defects in muscle mitochondria contribute to ALS. In this study, we further demonstrate that acutely expressed human SOD1 proteins reach inside muscle mitochondria, where the mutant SOD1 may exert a role in disrupting function (supplemental data 2). The toxicity of mutant SOD1 may be dose-dependent as partial reduction of the expression of mutant SOD1 in muscle did not affect the disease onset or survival in ALS transgenic mice (33).

It has been shown that elevated $[Ca^{2+}]_i$ could promote the aggregation of mutant SOD1 inside mitochondria and exacerbate the loss of $\Delta\Psi$ in cultured motor neurons (34). Although we did not detect an elevated $[Ca^{2+}]_i$ at rest, osmotic stress caused the area with defective mitochondria to display increased Ca^{2+} release activity, which could lead to a sustained elevation of $[Ca^{2+}]_i$ near the NMJ and accelerate mitochondrial defects near the defective region. Furthermore, nicotinic acetylcholine receptors are abundant in the postsynaptic membrane of the NMJ. There is evidence of an elevated Ca^{2+} permeability of the nicotinic acetylcholine receptors in adult mammalian muscle (35), and it has been found that nicotinic acetylcholine receptors are more numerous in G93A muscle (31). Thus, it can be expected that following repetitive stimulations, mitochondria near the NMJ will face elevated local $[Ca^{2+}]$ and thereby become more susceptible to the deleterious effects of the mutant SOD1. A similar Ca^{2+}-mediated mechanism may also apply to the neuronal side of the NMJ. Earlier studies by Siklós *et al.* (36) showed that motor nerve terminals from ALS specimens contained significantly increased levels of Ca^{2+}. It has also been demonstrated that repetitive action potentials increase cytosolic Ca^{2+} level rapidly and heavily load local mitochondria in motor terminals of G93A mice (37, 38). This may accelerate the mitochondrial damage induced by mutant SOD1 and axonal degeneration, which in turn would foster denervation and its consequences. However, this is only an inference by analogy, not based on specific studies on nerve cells.

Based on past and present results, one potential model of the pathogenic sequence in ALS skeletal muscle is depicted in Fig. 5. In early presymptomatic stages (Fig. 5*A*), the situation is sim-

ilar to the WT. Probably the abnormality at this stage is the accumulation of mutant SOD1 inside mitochondria, an event that may occur simultaneously in muscle and nerve terminals. Accumulation of these defects would result in compromised mitochondrial potential near the NMJ, which would reduce mitochondrial capacity for Ca^{2+} uptake and lead to abnormal Ca^{2+} release in this region (Fig. 5*B*). This abnormal release stresses neighboring normal mitochondria, causing a decrease in their $\Delta\Psi$ and furthering the elevation of $[Ca^{2+}]_i$ after the stimulation. In this view, the process of muscle degeneration may involve a dual interplay between abnormal mitochondria and uncontrolled SR Ca^{2+} release in both muscle fibers and nerve terminals, which eventually leads to destruction of both cells.

Mitochondrial Ca^{2+} uptake is believed to help regulate mitochondrial metabolism and synthesis of ATP so that the demands of muscle contraction are met. Whether mitochondrial Ca^{2+} uptake modifies Ca^{2+} signaling during excitation-contraction coupling remains an open question. A recent review summarized 70 publications supporting or arguing against this idea in cardiac muscle (39). In skeletal muscle, the situation is equally unsettled (reviewed in Ref. 15). Although studies show that mitochondria in skeletal muscle can take up Ca^{2+} during contraction (40, 41), it is not known whether altered mitochondrial Ca^{2+} uptake can play a role in pathophysiological conditions. By demonstrating increased local Ca^{2+} release in areas of mitochondrial deficiency, the stop of propagation of Ca^{2+} waves in the neighboring normal areas, and the exacerbation of some of these effects by interfering with mitochondrial Ca^{2+} uptake, our study constitutes a direct demonstration of the importance of mitochondria in shaping cytosolic Ca^{2+} signaling in skeletal muscle. Malfunction of mitochondrial Ca^{2+} uptake likely plays an important role in muscle degeneration of ALS. It must be noted that Ca^{2+} release was induced by osmotic shock, a nonphysiological stimulus in our experimental condition. Future studies are required to quantify the amplitude and kinetics of mitochondrial Ca^{2+} uptake during physiologic excitation-contraction coupling.

The present studies do not exclude other potential contributions to the abnormal Ca^{2+} transient in G93A muscle. A distinct possibility is that the increased Ca^{2+} level is a consequence of increased membrane permeability to Ca^{2+} in the area of lesion. In a study documented with supplemental data 1, we found that eliminating external Ca^{2+} did not stop the osmotic stress-induced hyperactive Ca^{2+} release in the area of lesion, which suggests that Ca^{2+} entry through the plasma membrane is not a major contributor to the elevated Ca^{2+} in the area with depolarized mitochondria. An enhanced Ca^{2+} release activity could also reflect functional changes in the SR or an altered production of reactive oxygen species. Future studies are required to elucidate the relative contribution of denervation *versus* a primary muscle effect due to SOD1 mutation in producing defective Ca^{2+} signaling and triggering the initial mitochondrial defect in ALS muscle.

In summary, the new data demonstrate that a localized mitochondrial lesion in skeletal muscle is an early event during the progression of ALS. Understanding this and other cellular events underlying muscle degeneration will facilitate the development of rational therapeutic approaches to ALS.

Acknowledgments—We thank Drs. L. A. Blatter (Rush University, Chicago, IL) and N. Weisleder (UMDNJ-Robert Wood Johnson Medical School, Piscataway, NJ) for valuable discussions on this manuscript.

REFERENCES

1. Pasinelli, P., and Brown, R. H. (2006) *Nat. Rev. Neurosci.* **7,** 710–723
2. Gurney, M. E., Pu, H., Chiu, A. Y., Dal Canto, M. C., Polchow, C. Y., Alexander, D. D., Caliendo, J., Hentati, A., Kwon, Y. W., and Deng, H. X. (1994) *Science* **264,** 1772–1775
3. Appel, S. H. (2006) *Exp. Neurol.* **198,** 1–3
4. Dupuis, L., di Scala, F., Rene, F., de Tapia, M., Oudart, H., Pradat, P. F., Meininger, V., and Loeffler, J. P. (2003) *FASEB J.* **17,** 2091–2093
5. Park, K. H., and Vincent, I. (2008) *Biochim. Biophys. Acta* **1782,** 462–468
6. Leclerc, N., Ribera, F., Zoll, J., Warter, J. M., Poindron, P., Lampert, E., and Borg, J. (2001) *Neuromuscul. Disord.* **11,** 722–727
7. Mahoney, D. J., Kaczor, J. J., Bourgeois, J., Yasuda, N., and Tarnopolsky, M. A. (2006) *Muscle Nerve* **33,** 809–816
8. Weisleder, N., Brotto, M., Komazaki, S., Pan, Z., Zhao, X., Nosek, T., Parness, J., Takeshima, H., and Ma, J. (2006) *J. Cell Biol.* **174,** 639–645
9. Payne, A. M., Jimenez-Moreno, R., Wang, Z. M., Messi, M. L., and Delbono, O. (2009) *Exp. Gerontol.* **44,** 261–273
10. Hopf, F. W., Turner, P. R., Denetclaw, W. F., Jr., Reddy, P., and Steinhardt, R. A. (1996) *Am. J. Physiol.* **271,** C1325–1339
11. De Backer, F., Vandebrouck, C., Gailly, P., and Gillis, J. M. (2002) *J. Physiol.* **542,** 855–865
12. Wang, X., Weisleder, N., Collet, C., Zhou, J., Chu, Y., Hirata, Y., Zhao, X., Pan, Z., Brotto, M., Cheng, H., and Ma, J. (2005) *Nat. Cell Biol.* **7,** 525–530
13. Han, R., Grounds, M. D., and Bakker, A. J. (2006) *Cell Calcium* **40,** 299–307
14. DiFranco, M., Woods, C. E., Capote, J., and Vergara, J. L. (2008) *Proc. Natl. Acad. Sci. U.S.A.* **105,** 14698–14703
15. Rossi, A. E., Boncompagni, S., and Dirksen, R. T. (2009) *Exerc. Sport Sci. Rev.* **37,** 29–35
16. Launikonis, B. S., Zhou, J., Royer, L., Shannon, T. R., Brum, G., and Ríos, E. (2005) *J. Physiol.* **567,** 523–543
17. Deng, H. X., Shi, Y., Furukawa, Y., Zhai, H., Fu, R., Liu, E., Gorrie, G. H., Khan, M. S., Hung, W. Y., Bigio, E. H., Lukas, T., Dal Canto, M. C., O'Halloran, T. V., and Siddique, T. (2006) *Proc. Natl. Acad. Sci. U.S.A.* **103,** 7142–7147
18. Wong, P. C., Pardo, C. A., Borchelt, D. R., Lee, M. K., Copeland, N. G., Jenkins, N. A., Sisodia, S. S., Cleveland, D. W., and Price, D. L. (1995) *Neuron* **14,** 1105–1116
19. Kong, J., and Xu, Z. (1998) *J. Neurosci.* **18,** 3241–3250
20. Martins, A. S., Shkryl, V. M., Nowycky, M. C., and Shirokova, N. (2008) *J. Physiol.* **586,** 197–210
21. Shkryl, V. M., Martins, A. S., Ullrich, N. D., Nowycky, M. C., Niggli, E., and Shirokova, N. (2009) *Pflugers Arch.* **458,** 915–928
22. Teichmann, M. D., Wegner, F. V., Fink, R. H., Chamberlain, J. S., Launikonis, B. S., Martinac, B., and Friedrich, O. (2008) *PLoS ONE* **3,** e3644
23. Zhou, J., Yi, J., Royer, L., Launikonis, B. S., González, A., García, J., and Ríos, E. (2006) *Am. J. Physiol. Cell Physiol.* **290,** C539–553
24. Zhou, J., Brum, G., Gonzalez, A., Launikonis, B. S., Stern, M. D., and Rios, E. (2003) *J. Gen. Physiol.* **122,** 95–114
25. Kirichok, Y., Krapivinsky, G., and Clapham, D. E. (2004) *Nature* **427,** 360–364
26. Matlib, M. A., Zhou, Z., Knight, S., Ahmed, S., Choi, K. M., Krause-Bauer, J., Phillips, R., Altschuld, R., Katsube, Y., Sperelakis, N., and Bers, D. M. (1998) *J. Biol. Chem.* **273,** 10223–10231
27. Buntinas, L., Gunter, K. K., Sparagna, G. C., and Gunter, T. E. (2001) *Biochim. Biophys. Acta* **1504,** 248–261
28. Fischer, L. R., Culver, D. G., Tennant, P., Davis, A. A., Wang, M., Castellano-Sanchez, A., Khan, J., Polak, M. A., and Glass, J. D. (2004) *Exp. Neurol.* **185,**

232–240
29. Nguyen, Q. T., Son, Y. J., Sanes, J. R., and Lichtman, J. W. (2000) *J. Neurosci.* **20,** 6077–6086
30. Funakoshi, H., Belluardo, N., Arenas, E., Yamamoto, Y., Casabona, A., Persson, H., and Ibáñez, C. F. (1995) *Science* **268,** 1495–1499
31. Dobrowolny, G., Giacinti, C., Pelosi, L., Nicoletti, C., Winn, N., Barberi, L., Molinaro, M., Rosenthal, N., and Musarò, A. (2005) *J. Cell Biol.* **168,** 193–199
32. Dobrowolny, G., Aucello, M., Rizzuto, E., Beccafico, S., Mammucari, C., Boncompagni, S., Bonconpagni, S., Belia, S., Wannenes, F., Nicoletti, C., Del Prete, Z., Rosenthal, N., Molinaro, M., Protasi, F., Fanò, G., Sandri, M., and Musarò, A. (2008) *Cell Metab.* **8,** 425–436
33. Miller, T. M., Kim, S. H., Yamanaka, K., Hester, M., Umapathi, P., Arnson, H., Rizo, L., Mendell, J. R., Gage, F. H., Cleveland, D. W., and Kaspar, B. K. (2006) *Proc. Natl. Acad. Sci. U.S.A.* **103,** 19546–19551
34. Kim, H. J., Im, W., Kim, S., Kim, S. H., Sung, J. J., Kim, M., and Lee, K. W. (2007) *Exp. Mol. Med* **39,** 574–582
35. Fucile, S. (2004) *Cell Calcium* **35,** 1–8
36. Siklós, L., Engelhardt, J. I., Alexianu, M. E., Gurney, M. E., Siddique, T., and Appel, S. H. (1998) *J. Neuropathol. Exp. Neurol* **57,** 571–587
37. Vila, L., Barrett, E. F., and Barrett, J. N. (2003) *J. Physiol.* **549,** 719–728
38. Nguyen, K. T., García-Chacón, L. E., Barrett, J. N., Barrett, E. F., and David, G. (2009) *Proc. Natl. Acad. Sci. U.S.A.* **106,** 2007–2011
39. O'Rourke, B., and Blatter, L. A. (2009) *J. Mol. Cell Cardiol.* **46,** 767–774
40. Rudolf, R., Mongillo, M., Magalhães, P. J., and Pozzan, T. (2004) *J. Cell Biol.* **166,** 527–536
41. Bruton, J., Tavi, P., Aydin, J., Westerblad, H., and Lännergren, J. (2003) *J. Physiol.* **551,** 179–190